

Quantum dynamics study of H exchange reaction of $\text{H}'(^2\text{S}) + \text{CH}(X^2\Pi) \rightarrow \text{H}(^2\text{S}) + \text{CH}'(X^2\Pi)$ and Isotope Reactions of $\text{H}(^2\text{S}) + \text{CH}(X^2\Pi) \rightarrow \text{C}(^1\text{D}) + \text{H}_2(X^1\Sigma_g^+)$

Yunhui Wang, Kaiming Deng, and Ruifeng Lu^{a*}

Department of Applied Physics, Nanjing University of Science and Technology, Nanjing 210094, China

Received 30 December 2014; Accepted (in revised version) 15 February 2015

Published Online 1 March 2015

Abstract. By using the time-dependent quantum wave packet method, we report a detailed dynamics study of H exchange reaction $\text{H}'(^2\text{S}) + \text{CH}(X^2\Pi) \rightarrow \text{H}(^2\text{S}) + \text{CH}'(X^2\Pi)$ and the isotope effects of $\text{H}(^2\text{S}) + \text{CH}(X^2\Pi) \rightarrow \text{C}(^1\text{D}) + \text{H}_2(X^1\Sigma_g^+)$ reaction on the 11A BHL potential energy surface. The reaction probabilities and integral cross sections have been obtained for the initial states $v = 0$ and $j = 1$ of the reactant molecules. The dense resonance structures in the reaction probabilities at all total angular momenta indicate complex-forming mechanisms for both $\text{C} + \text{H}_2$ and $\text{H} + \text{CH}$ products. A comparison between the results from centrifugal sudden approximation and those from close-coupled calculations demonstrates that the Coriolis coupling effects get more and more pronounced with increasing of J for both H exchange reaction and CH decay reaction. The isotopic D substitution of reactant significantly influences the CH decay reaction. Moreover, it is revealed that the dynamical features such as partial wave contributions to the cross section are substantially different for these two channels.

PACS: 82.20.Fd, 71.15.Pd

Key words: time-dependent quantum wave packet, isotope effects, stereodynamics.

1 Introduction

Methylene molecule is an important intermediate in many organic reactions. It also plays an important role in astrochemical and combustion processes. As a prototype insertion reaction, $\text{C} + \text{H}_2 \rightarrow \text{H} + \text{CH}$ has drawn a great deal of attention in both experiments and theory, indicating that the reaction proceeds via the CH_2 intermediate which lives

*Corresponding author. *Email address:* rflu@njust.edu.cn (R.-F. Lu)

sufficiently long to permit complete energy randomization. So far, many experimental investigations of the CH₂ system have been done in understanding the kinetics [1] and dynamics [2-6]. The rotational state distribution of CH was measured and the reaction C(¹D) + H₂ was concluded to proceed via insertion of C(¹D) into the H-H bond in a facile manner.² The product angular distribution measured in a molecular beam experiment shows a backward-forward symmetry, suggesting the dominance of a long-lived CH₂ complex [3]. Isotope effect has been studied for the C(¹D) + H₂ reaction by Fisher and co-workers, who measured the CD/CH branching ratio and estimated the thermal rate constants for reactions C(¹D) + H₂/D₂ [4]. The product CH is found to be highly rotationally excited, and the -doublet and spin-orbit components are equally populated in the reaction C(¹D) + H₂ [5]. The CH rotational distribution was also observed from C(¹D) + H₂ collision by laser-induced fluorescence [6], which shows that only a small fraction of the CH product is formed in its vibrationally excited state. In this experiment, insertion is the major reaction mechanism, however, the abstraction process seems to be enhanced when the vibrational quantum number of CH product varies from 0 to 1. The rate constants at the room temperature were measured for the collisions of C(¹D) with H₂, HD and D₂ by standard pump-probe techniques, and the rotational distributions of CH and CD products as well as the branching ratio of CD/CH were also studied, suggesting that the long-lived complex HCH/D is formed during the reaction [7]. Moreover, the product angular and time-of-flight distributions for the reaction C(¹D) + H₂ were obtained by the crossed beam technique with mass spectrometric detection at the collision energy of 0.08 eV, which are in qualitative agreement with the statistical predication that the C + H₂ reaction behaves nearly statistically owing to the potential well is very deep [8].

The C(¹D) + H₂ reaction and its isotopic variants have also been intensively studied from the theoretical side. An adiabatic global potential energy surface (PES) for the first singlet state (1¹A') of CH₂ system has been built by Bussery-Honvault and co-workers (BHL PES), using multireference single and double configuration interaction calculations to characterize the state [9]. As depicted schematically in Fig. 1 of the BHL PES, for the H exchange reaction H'(²S) + CH(X²Π) → H(²S) + CH'(X²Π) and the CH decay reaction H(²S) + CH(X²Π) → C(¹D) + H₂(X¹Σ_g⁺), there exists a potential well with a depth of about 4.15 and 4.32 eV, corresponding to the H(²S) + CH(X²Π) and C(¹D) + H₂(X¹Σ_g⁺) asymptotes, respectively, located at R_{CH} = 2.09a₀ and θ_{HCH} = 102.5° in the internal coordinates. In addition, there is a relatively larger barrier of 0.54 eV in the collinear abstraction channel. A lot of achievements have been made by the quantum mechanical (QM) and quasi-classical trajectory (QCT) methods [9-17]. based on the BHL PES. Later, Bãnares and co-workers constructed a new form of the 1¹A' PES using the Reproducing Kernel Hilbert Space (RKHS) interpolation method [18]. The new PES is free of spurious scale feature compared to the original BHL PES, and the dynamics of C(¹D) + H₂ and its isotope reactions have been studied by accurate close-coupled (CC) QM methods on the RKHS PES [19-23]. Also, a single sheeted double many-body expansion (DMBE) PES was reported by fitting accurate ab initio energies from the multireference configuration interaction method for the 1¹A' state of CH₂ [24], and the energies are corrected by the

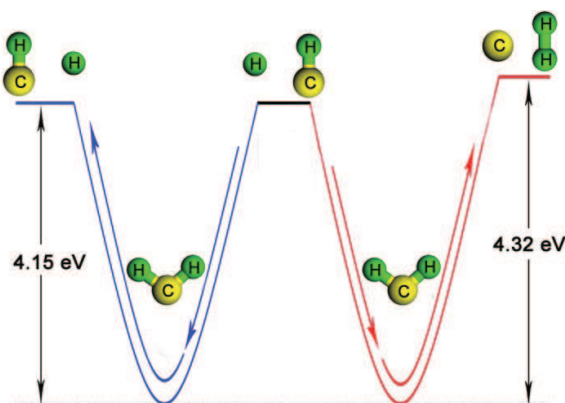


Figure 1: Schematic diagram of the PES for two reactive channels, $\text{H}'(^2\text{S}) + \text{CH}(X^2\Pi) \rightarrow \text{H}(^2\text{S}) + \text{CH}'(X^2\Pi)$ (left) and $\text{H}(^2\text{S}) + \text{CH}(X^2\Pi) \rightarrow \text{C}(^1\text{D}) + \text{H}_2(X^1\Sigma_g^+)$ (right).

DMBE scaled external correlation method to mimic full configuration interaction [25-30]. The DMBE PES has a well depth of 4.34 eV to the $\text{C}(^1\text{D}) + \text{H}_2$ asymptote, which is close to the previous BHL PES. QCT calculations for the $\text{C}(^1\text{D}) + \text{H}_2/\text{HD}/\text{D}_2$ reactions have been performed on the DMBE PES, and the calculated integral cross sections (ICs) agree well with the available theoretical [13,17,18,21-23,31-33] and experimental [7] data.

All above works are referred to the forward insertion reaction $\text{C} + \text{H}_2 \rightarrow \text{H} + \text{CH}$, and the reaction dynamics has been well understood based on different PESs and methods. To our knowledge, the reverse reaction, $\text{H}(^2\text{S}) + \text{CH}(X^2\Pi) \rightarrow \text{C}(^3\text{P}) + \text{H}_2(X^1\Sigma_g^+)$, has been investigated carefully in experiments [34-36] and theory [34-39], however, the $\text{H}(^2\text{S}) + \text{CH}(X^2\Pi)$ reaction has not been entirely explored. The latter collision capable of sustaining a long-lived complex attracts us to present more physical and chemical dynamics information of the two reactive channels $\text{H}'(^2\text{S}) + \text{CH}(X^2\Pi) \rightarrow \text{H}(^2\text{S}) + \text{CH}'(X^2\Pi)$ and $\text{H}(^2\text{S}) + \text{CH}(X^2\Pi) \rightarrow \text{C}(^1\text{D}) + \text{H}_2(X^1\Sigma_g^+)$.

2 Theoretical methods

In this work, time-dependent quantum wave packet method is employed to numerically calculate dynamical properties of the title reactions on BHL PES. The general theory of this well-known QM method is standard and referred to the published literatures [40-44]. The following parameters were taken to get the converged results: In the reactant Jacobi coordinates, 210 translational basis functions for R grids in the range of 0.1 to 15.0 $a.u.$ and 100 vibrational basis functions for r grids in the range of 0.5 to 11.5 $a.u.$ were used. The total propagation time is 35000 $a.u.$, and j_{max} is chosen to be 80 for rotational basis functions. We have carried out the calculations with both centrifugal sudden (CS) approximation and CC (including the Coriolis coupling) method for comparison, and the number of the projection of total angular momentum on the body-fixed z -axis is up to 5

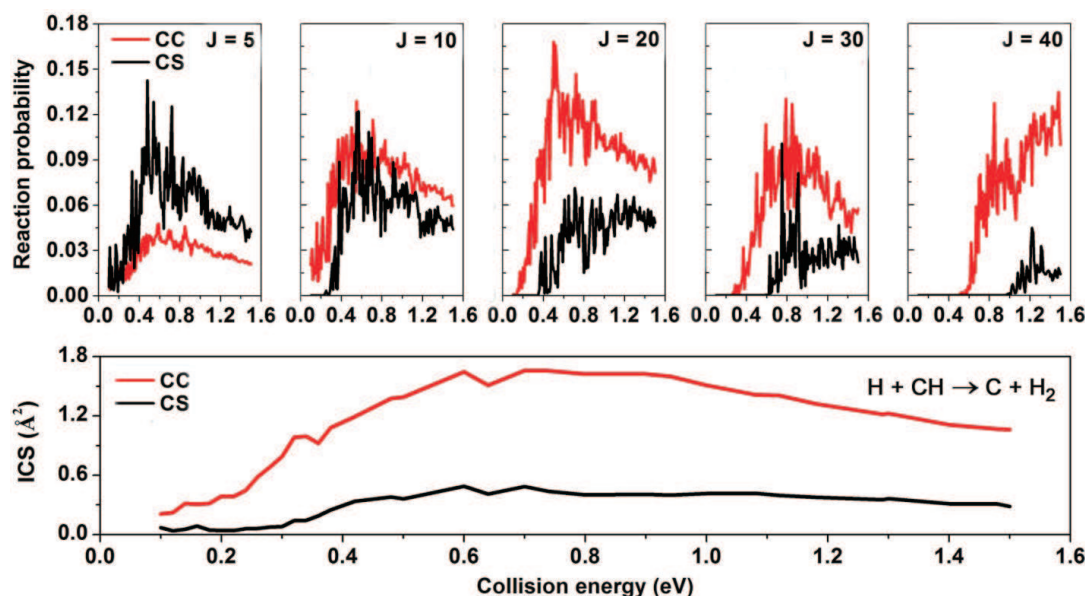


Figure 2: The CC and CS probabilities for total angular momentum $J = 5, 10, 20, 30,$ and $40,$ and the CC and CS ICSs for $\text{H}(\text{S}) + \text{CH}(\text{X}^2\Pi; v = 0, j = 1) \rightarrow \text{C}(\text{D}) + \text{H}_2(\text{X}^1\Sigma_g^+)$ reaction.

in the CC calculations. Due to that the lowest allowed rotational state of $\text{CH}(\text{X}^2\Pi)$ is $j = 1,$ we use the ground vibrational level and the minimal allowed rotational level of the reactant molecule throughout the paper.

3 Results and discussion

3.1 Coriolis coupling effect in $\text{H}(\text{S}) + \text{CH}(\text{X}^2\Pi) \rightarrow \text{C}(\text{D}) + \text{H}_2(\text{X}^1\Sigma_g^+)$ reaction

Coriolis coupling effect, being an intramolecular process, can exist with its influence on the relevant phenomena occurring in colliding chemical reaction process, which plays an important role in understanding the reaction dynamic processes. Fig. 2 shows the CC and CS probabilities for the initial quantum numbers $v = 0, j = 1$ of CH, and the total angular momentum J of 5, 10, 20, 30, and 40. We can see the resonance peaks are very intense and sharp which are associated with the intermediate complex due to the deep well in the PES. With the increasing of the total angular momentum $J,$ the difference between the two sets of calculations becomes larger, and the overall curves shift to high-energy part with a relatively slower shifting for CC calculations. More specifically, for low J values, such as $J = 5,$ the calculated CC probability is lower than that from CS calculations, however, for $J = 10,$ the CC probability is larger than the CS one although the differences between them are rather small at some collision energies. As for $J = 20, 30,$ and $40,$ the significant differences are observed, and the CC values are always larger than

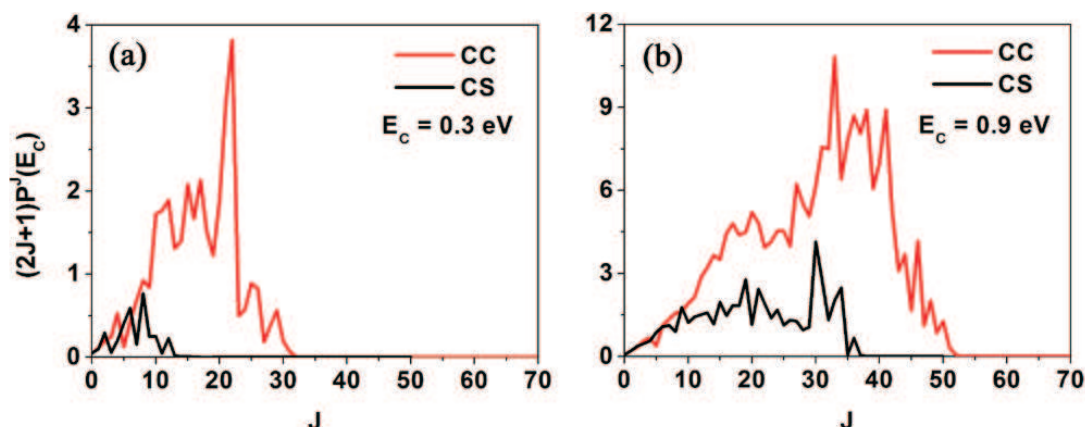


Figure 3: Weighted partial wave contributions to the ICS of $\text{H}(^2\text{S}) + \text{CH}(X^2\Pi; v = 0, j = 1) \rightarrow \text{C}(^1\text{D}) + \text{H}_2(X^1\Sigma_g^+)$ reaction at two collision energies (a) $E_c = 0.3$ eV and (b) $E_c = 0.9$ eV.

the CS ones in the whole collision energy range. In fact, neglecting Coriolis coupling in the CS approximation confines the molecular rotation to the molecular plane. When the long-lived complex is formed, out-of-plane rotations (molecules rotating in various directions) are excluded by the CS approximation, which can prompt the vibrational modes advantageous for the bond breaking of the complex and thus excite the product formation during the collision. The similar phenomenon and conclusion are obtained in the dynamics of $\text{He} + \text{H}_2^+$ [45]. Furthermore, it can be seen that the CC reaction probability is initially becoming higher until $J = 20$ and then falls off, while only a monotonous decreasing trend is found for the CS calculations. By comparing the CC and CS results, it is obvious that the effect of Coriolis coupling on the CH decay reaction with a deep well on the ground state PES is remarkable, thus neglecting the Coriolis coupling is inappropriate in accurate dynamics studies. This impression is further reinforced from the comparison of the ICSs in Fig. 2.

Unlike the reaction probability curve, no intense resonance peaks appear in the ICSs owing to the J -averaging effect. Although both the CC and CS cross sections have a similar trend as a function of collision energy (specifically, the ICSs first increase rapidly at low collision energies and reach a maximum, then decline at high collision energies), the CC ICS is always larger than the CS one with a maximum difference of 5 times in the collision energy range from 0.3 to 1.5 eV. Thus, the total ICS is severely underestimated by neglecting the Coriolis coupling. The large differences of ICSs between CC and CS calculations once again indicate that the Coriolis coupling should be considered in the reaction dynamics study for this reaction system.

In Fig. 3, we present J -dependent partial wave contributions to the ICSs at two collision energies of 0.3 eV and 0.9 eV. From the comparison between the CC and CS results, we can infer that the Coriolis coupling has relatively small influence for low J , nevertheless, it can not be ignored with increasing J . The CC calculations usually give much

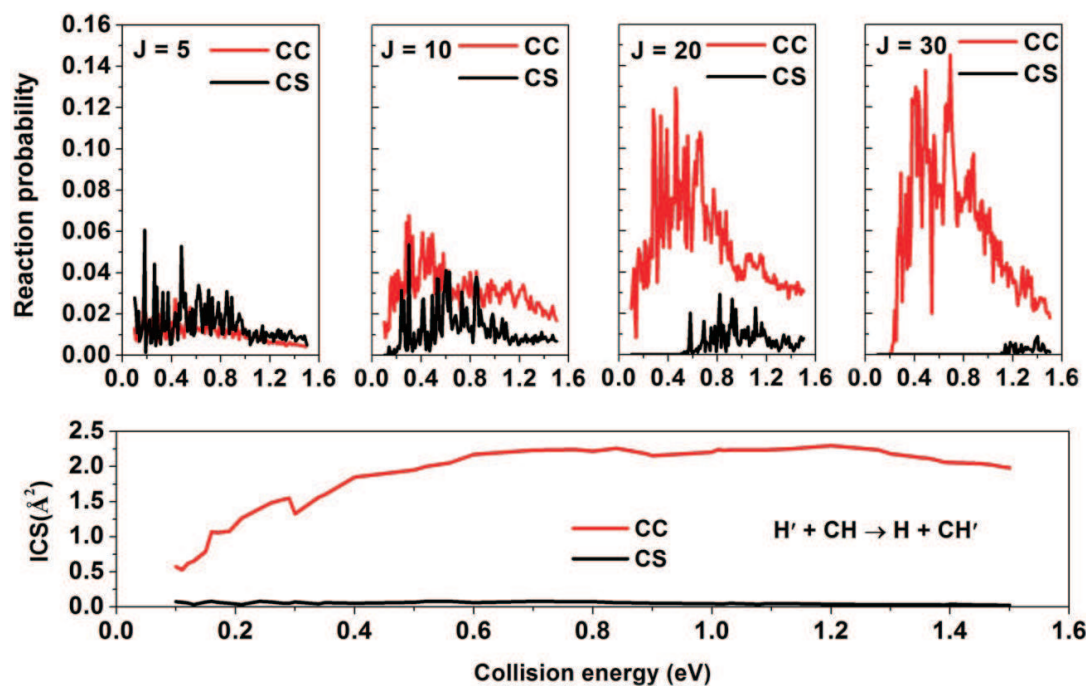


Figure 4: The CC and CS probabilities for $J = 5, 10, 20, 30$ and 40 , and the CC and CS ICSs for the H exchange reaction $\text{H}'(^2\text{S}) + \text{CH}(X^2\Pi; v = 0, j = 1) \rightarrow \text{H}(^2\text{S}) + \text{CH}'(X^2\Pi)$.

more contribution to the ICS for higher J because rotating effects in various directions for the reagent molecules are taken into account, and the trend is very obvious at the low collision energy.

3.2 H exchange reaction $\text{H}'(^2\text{S}) + \text{CH}(X^2\Pi) \rightarrow \text{H}(^2\text{S}) + \text{CH}'(X^2\Pi)$

In this section, we studied the dynamical feature as well as the Coriolis coupling effect of the H exchange channel from the $\text{H}(^2\text{S}) + \text{CH}(X^2\Pi)$ collision. The isolation of $\text{H}'(^2\text{S}) + \text{CH}(X^2\Pi) \rightarrow \text{H}(^2\text{S}) + \text{CH}'(X^2\Pi)$ from other channels can be realized by performing the flux analysis [38]. The H exchange reaction also undergoes the deep well and sustains a long-lived complex of H-C-H as shown in Fig. 1. Fig. 4 illustrates the CC and CS reaction probabilities for $J = 5, 10, 20$ and 30 in the collision energy range from 0.1 eV to 1.5 eV. At low total angular momentum, such as $J = 5$, the differences between CC and CS calculated probabilities are small. However, the CS probability is always smaller than the CC one, and the performance of CS calculations gets worse gradually that the CS probability decreases monotonously as J increases whereas the CC one increases until $J = 63$.

We also depict the CC and CS ICSs as a function of collision energy in Fig. 4. The dramatic differences between CC and CS ICSs indicate that the Coriolis coupling effect must be carefully considered in the H exchange reaction. In addition, an adiabatic dynamics

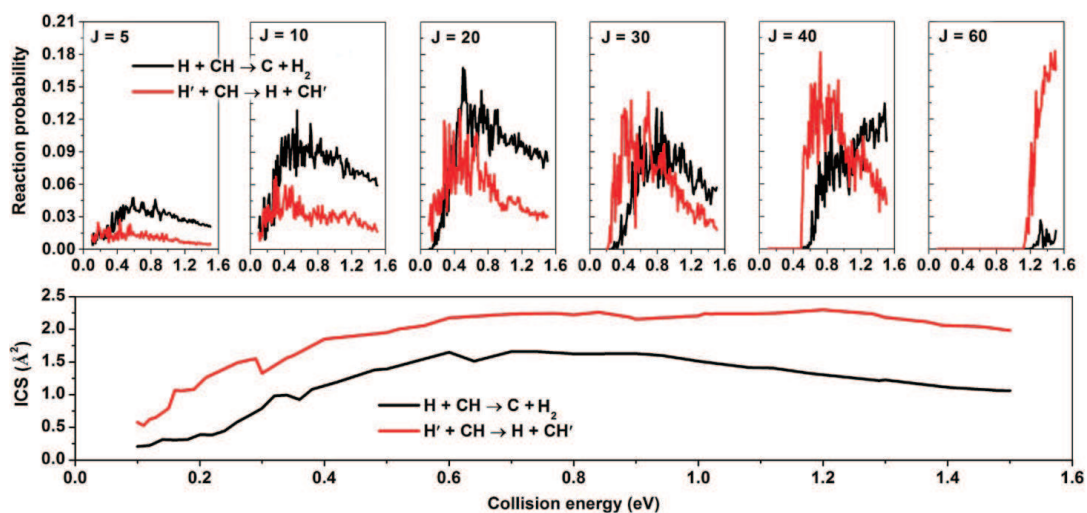


Figure 5: The CC probabilities for total angular momentum $J = 5, 10, 20, 30$ and 40 , and the CC ICSs of the $\text{H}(^2\text{S}) + \text{CH}(X^2\Pi; v = 0, j = 1) \rightarrow \text{C}(^1\text{D}) + \text{H}_2(X^1\Sigma_g^+)$ reaction and $\text{H}'(^2\text{S}) + \text{CH}(X^2\Pi; v = 0, j = 1) \rightarrow \text{H}(^2\text{S}) + \text{CH}'(X^2\Pi)$ reaction.

study of $\text{H} + \text{O}_2$ via a deep potential well has demonstrated that the Coriolis coupling becomes more and more important with increasing J and collision energy [46-48]. Moreover, Coriolis coupling effect in some nonadiabatic [49-50] processes has been proved very essential. Since the importance of Coriolis coupling has been revealed for accurate describing the dynamical behavior of the CH decay reaction and H exchange reaction, we only present the CC results in the following.

Fig. 5 shows the CC reaction probabilities and ICSs for two reactive channels $\text{H}(^2\text{S}) + \text{CH}(X^2\Pi) \rightarrow \text{C}(^1\text{D}) + \text{H}_2(X^1\Sigma_g^+)$ and $\text{H}'(^2\text{S}) + \text{CH}(X^2\Pi) \rightarrow \text{H}(^2\text{S}) + \text{CH}'(X^2\Pi)$. At low J values, the reaction probabilities for the two channels have small differences in the low collision energy region. At very high collision energies, large discrepancy between two channels are observed, and the probabilities of the $\text{CH}(X^2\Pi)$ decay channel are always bigger than those of the H exchange channel with J increasing until $J = 60$, which indicates that the higher collision energy makes the $\text{C} + \text{H}_2$ product more accessible. It is clear that the exchange reaction is the dominant process at very low collision energies for $J = 20, 30$ and 40 . From the ICSs curves, we can see that H exchange reaction occurs more easily than the $\text{H}(^2\text{S}) + \text{CH}(X^2\Pi) \rightarrow \text{C}(^1\text{D}) + \text{H}_2(X^1\Sigma_g^+)$ channel in the whole considered collision energy range.

To gain more insights into the reaction dynamics for the $\text{H}(^2\text{S}) + \text{CH}(X^2\Pi)$ collision, we plot the J -dependent partial wave contributions to the ICSs at three collision energies of 0.6 eV, 0.9 eV and 1.2 eV in Fig. 6. With the increasing of collision energy, the positions of the main resonance peak move to higher J , for both channels. The resonance features are not fully washed out after summing over J in the determination of the ICS. The main envelopes of the partial wave contributions are obviously different for these two chan-

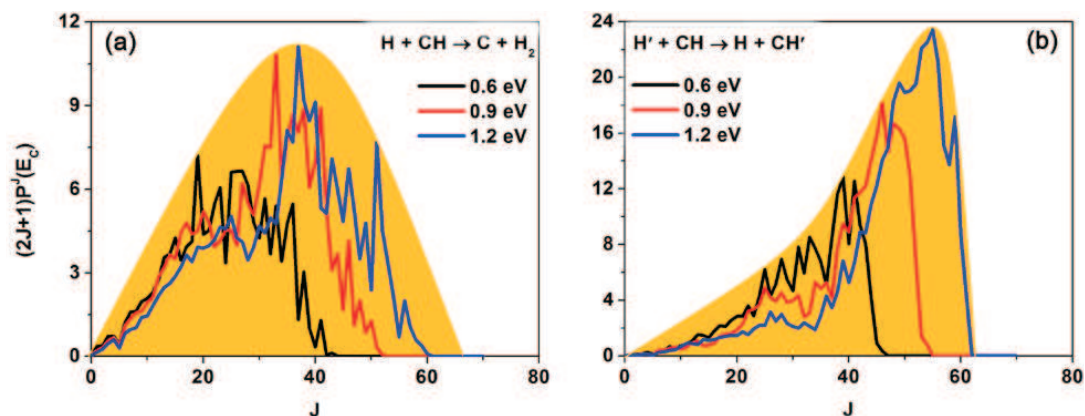


Figure 6: Weighted partial wave contributions to the ICS of the (a) $\text{H}(^2\text{S}) + \text{CH}(\text{X}^2\Pi; v = 0, j = 1) \rightarrow \text{C}(^1\text{D}) + \text{H}_2(\text{X}^1\Sigma_g^+)$ reaction and (b) $\text{H}'(^2\text{S}) + \text{CH}(\text{X}^2\Pi; v = 0, j = 1) \rightarrow \text{H}(^2\text{S}) + \text{CH}'(\text{X}^2\Pi)$ reaction as a function of total angular momentum J at four collision energies $E_c = 0.3$ eV, 0.6 eV, 0.9 eV, and 1.2 eV.

nels, and there is a strong high- J preference in the partial wave contributions to the ICSs for the H exchange channel, in comparison with that the major contribution originates from the intermediate J among all the partial waves for the CH decay reaction.

3.3 Isotope effects on the $\text{H}(^2\text{S}) + \text{CH}(\text{X}^2\Pi) \rightarrow \text{C}(^1\text{D}) + \text{H}_2(\text{X}^1\Sigma_g^+)$ reaction

In the present section, we will discuss the isotope effects on the dynamics of CH decay reaction. The H + CH, H + CD, D + CH and D + CD collisions are considered in our CC calculations. Consequently, we will pay attention to two kinds of isotopic substitutions: (I) the H of the CH molecule is substituted by D, such as H + CD reaction; (II) the H atom is replaced by D, such as D + CH reaction.

Fig. 7 displays the reaction probabilities for H + CH/CD and D + CH/CD with selected J values and ICSs from accurate CC calculations, respectively. As shown in the figure, the reaction probability gets increased at low $J = 5$ after the isotopic substitution in the molecular CH for H + CH reaction, however, opposite tendency can be observed with J increasing. It is worth noting that the reaction probability of reaction H + CH increases to a maximum at $J = 20$ at almost collision energies and then decreases with continuous increasing of J , however, the probability for isotopic variant H + CD presents a monotonous decreasing trend. A similar trend can be clearly found for both D + CH and D + CD reactions, that is, the reaction probability increases to the maximum at $J = 20$ following a decline with the increasing of J . However, the reaction probability of the $\text{D}(^2\text{S}) + \text{CD}(\text{X}^2\Pi) \rightarrow \text{C}(^1\text{D}) + \text{D}_2(\text{X}^1\Sigma_g^+)$ reaction is always larger than that of $\text{D}(^2\text{S}) + \text{CH}(\text{X}^2\Pi) \rightarrow \text{C}(^1\text{D}) + \text{HD}(\text{X}^1\Sigma_g^+)$ except for few resonance peaks at intermediate collision energy. Due to the J -averaging effect, the pronounced resonances in the reaction probability curves are greatly suppressed in the ICSs. From Fig. 7, we know that the reaction probability of H + CH reaction is smaller than the corresponding probability of its isotope reaction H + CD at low collision energies, leading to an intersection in ICSs at 0.5

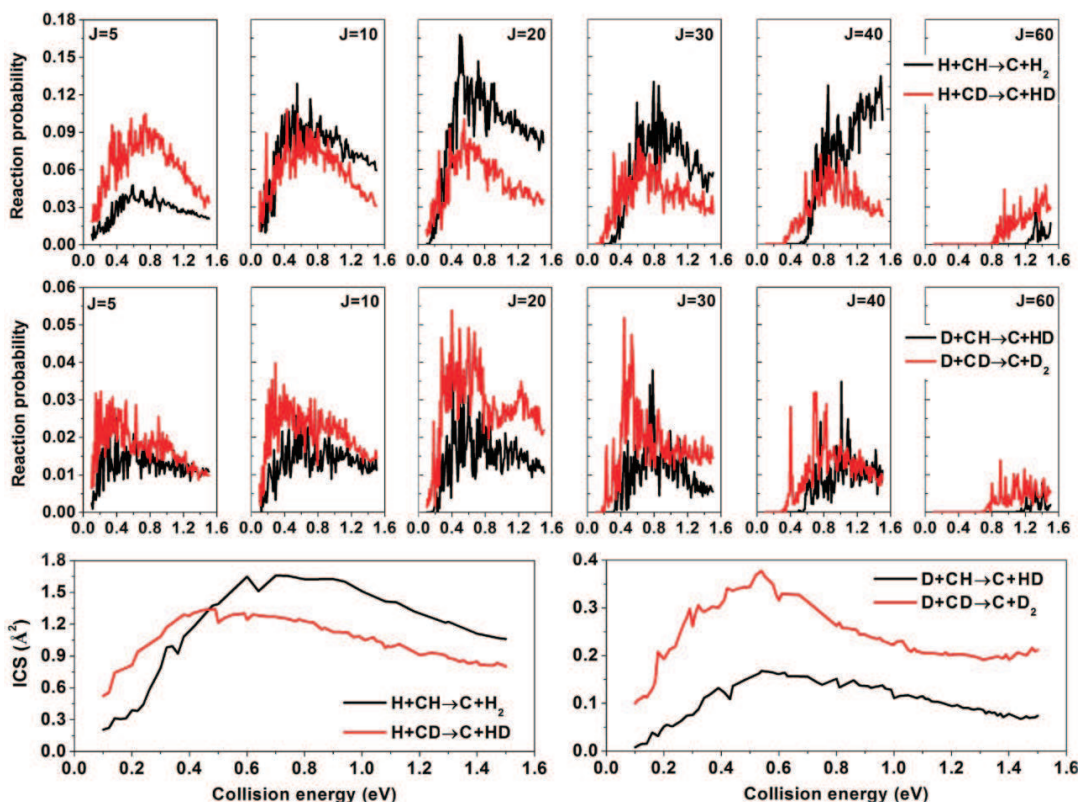


Figure 7: Comparisons of probabilities and ICSs between the $\text{H}(^2\text{S}) + \text{CH}(X^2\Pi; v=0, j=1) \rightarrow \text{C}(^1\text{D}) + \text{H}_2(X^1\Sigma_g^+)$ and $\text{H}(^2\text{S}) + \text{CD}(X^2\Pi; v=0, j=1) \rightarrow \text{C}(^1\text{D}) + \text{HD}(X^1\Sigma_g^+)$, and between the $\text{D}(^2\text{S}) + \text{CH}(X^2\Pi; v=0, j=1) \rightarrow \text{C}(^1\text{D}) + \text{HD}(X^1\Sigma_g^+)$ and $\text{D}(^2\text{S}) + \text{CD}(X^2\Pi; v=0, j=1) \rightarrow \text{C}(^1\text{D}) + \text{D}_2(X^1\Sigma_g^+)$ reactions.

eV. For heavy D collides with CH, we note that its ICS increases remarkably in the whole collision energy range by isotopic substituting with molecular CD.

By reconstructing the above results, we can also examine the type II isotope effect, i.e., the atomic H not the chemically bonded H is substituted by heavier D. In Fig. 8, the reaction probability of the H + CH reaction is always larger than that of D + CH, and the difference between them becomes more and more remarkable with J increased, which means the isotopic substitution of the colliding H atom will impede the CH decay, as further illustrated from the ICSs. A comparison of reaction probability and ICSs between the H + CD and D + CD reactions depicted in Fig. 8 also indicates that the isotopic substitution of H atom will impede the CD decay.

4 Conclusions

In summary, we have performed quantum scattering calculations on the BHL PES to study the dynamics of the H exchange reaction and colliding CH molecule decay reac-

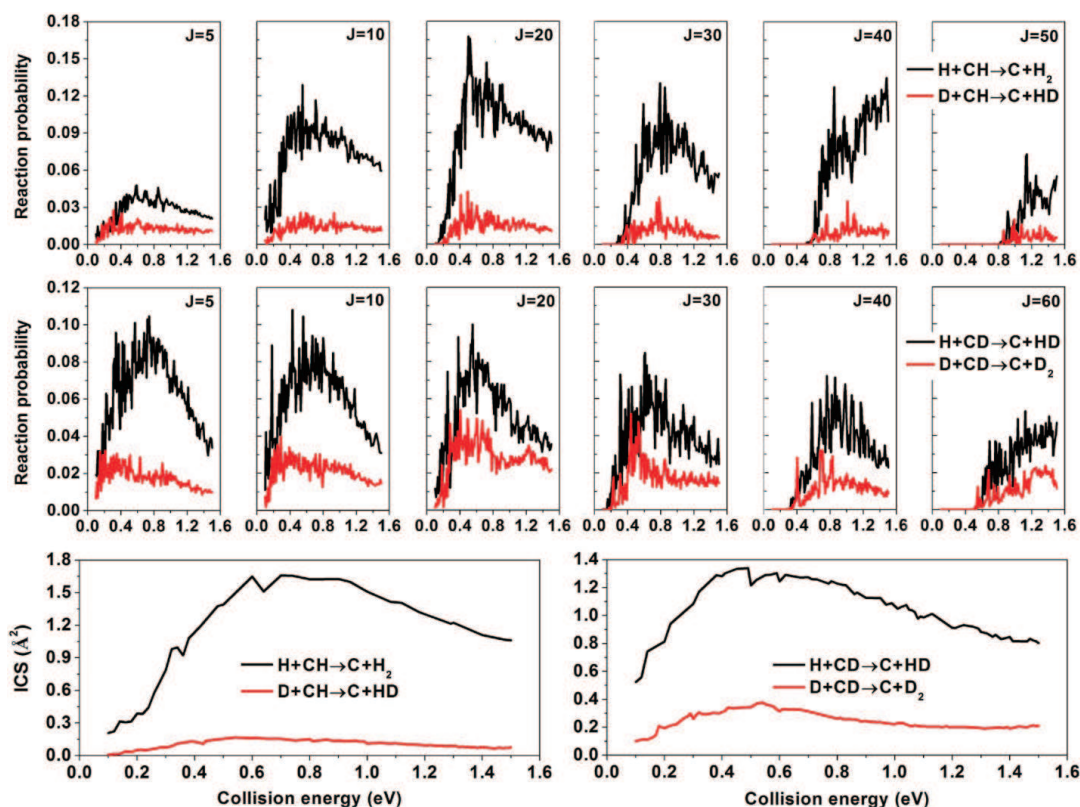


Figure 8: Comparisons of probabilities and ICSs between the $\text{H}(^2\text{S}) + \text{CH}(X^2\Pi; v = 0, j = 1) \rightarrow \text{C}(^1\text{D}) + \text{H}_2(X^1\Sigma_g^+)$ and $\text{D}(^2\text{S}) + \text{CH}(X^2\Pi; v = 0, j = 1) \rightarrow \text{C}(^1\text{D}) + \text{HD}(X^1\Sigma_g^+)$, and between the $\text{H}(^2\text{S}) + \text{CD}(X^2\Pi; v = 0, j = 1) \rightarrow \text{C}(^1\text{D}) + \text{HD}(X^1\Sigma_g^+)$ and $\text{D}(^2\text{S}) + \text{CD}(X^2\Pi; v = 0, j = 1) \rightarrow \text{C}(^1\text{D}) + \text{D}_2(X^1\Sigma_g^+)$ reactions.

tion as well as the isotope effects of the latter reactive channel. Detailed comparisons between the collision-energy-dependent CC and CS reaction probabilities and ICSs for both $\text{H}(^2\text{S}) + \text{CH}(X^2\Pi) \rightarrow \text{H}(^2\text{S}) + \text{CH}'(X^2\Pi)$ and $\text{H}(^2\text{S}) + \text{CH}(X^2\Pi) \rightarrow \text{C}(^1\text{D}) + \text{H}_2(X^1\Sigma_g^+)$ reactions reveal strong Coriolis coupling effects in $\text{H}(^2\text{S}) + \text{CH}(X^2\Pi)$ collisional reactions. The alternative H isotopic substitutions have been studied in colliding molecule decay reaction, and isotope effects are found to be pronounced in the calculated chemical dynamics quantities.

Acknowledgments This work was supported by the Fundamental Research Funds for the Central Universities (No. 30920140111008), NSF of China Grant (No. 11004107 and 21373113), and the Scientific Research Innovation Projects of Jiangsu Province for University Graduate Students with Grant No. CXZZ13_0201.

References

- [1] D. Husain and P. E. Norris, Faraday Discuss. Chem. Soc. 67, 273 (1979).

- [2] G. M. Jursich and J. R. Wiesenfeld, *Chem. Phys. Lett.* 110, 14 (1984).
- [3] A. Bergeat, L. Cartechini, N. Balucani, G. Capozza, L. F. Phillips, P. Casavecchia, G. G. Volpi, L. Bonnet, and J. C. Rayez, *Chem. Phys. Lett.* 327, 197 (2000).
- [4] W. H. Fisher, T. Carrington, C. M. Sadowski, and C. H. Dugan, *Chem. Phys.* 97, 433 (1985).
- [5] D. C. Scott, J. De Juan, D. C. Robie, D. Schwartz-Lavi, and H. Reisler, *J. Phys. Chem.* 96, 2509 (1992).
- [6] K. Mikulecky and K.-H. Gericke, *J. Chem. Phys.* 98, 1244 (1993).
- [7] K. Sato, N. Ishida, T. Kurakata, A. Iwasaki, and S. Tsuneyuki, *Chem. Phys. Lett.* 237, 195 (1998).
- [8] A. Bergeat, L. Cartechini, N. Balucani, G. Capozza, L. F. Phillips, P. Casavecchia, G. G. Volpi, L. Bonnet, and J.-C. Rayez, *Chem. Phys. Lett.* 327, 197 (2000).
- [9] B. Bussery-Honvault, P. Honvault, and J. M. Launay, *J. Chem. Phys.* 115, 10701 (2001).
- [10] N. Balucani, G. Capozza, L. Cartechini, A. Bergeat, R. Bobbenkamp, P. Casavecchia, F. J. Aoiz, L. Bãnares, P. Honvault, B. Bussery-Honvault, and J. M. Launay, *Phys. Chem. Chem. Phys.* 6, 4957 (2004).
- [11] N. Balucani, G. Capozza, E. Segoloni, R. Bobbenkamp, P. Casavecchia, T. Gonzalez-Lezana, E. J. Rackham, L. Bãnares, and J. F. Aoiz, *J. Chem. Phys.* 122, 234309 (2005).
- [12] L. Bãnares, F. J. Aoiz, P. Honvault, B. Bussery-Honvault, and J. M. Launay, *J. Chem. Phys.* 118, 565 (2003).
- [13] F. Gogtas, N. Bulut, and S. Akpınar, *Int. J. Quantum Chem.* 105, 478 (2005).
- [14] F. J. Aoiz, L. Bãnares, and V. J. Herrero, *J. Phys. Chem. A* 110, 12546 (2006).
- [15] L. H. Kang, *Int. J. Quant. Chem.* 111, 117 (2011).
- [16] L. H. Kang and B. Dai, *Can. J. Chem.* 88, 453 (2010).
- [17] L. H. Kang and M. Y. Zhu, *J. Mol. Struct.: THEOCHEM.* 945, 116 (2010).
- [18] L. Bãnares, F. Aoiz, S. A. Vázquez, T. S. Ho, and H. Rabitz, *Chem. Phys. Lett.* 374, 243 (2003).
- [19] S. Y. Lin and H. Guo, *J. Chem. Phys.* 120, 9907 (2004).
- [20] S. Y. Lin and H. Guo, *J. Chem. Phys.* 119, 11602 (2003).
- [21] S. Y. Lin and H. Guo, *J. Chem. Phys.* 121, 1285 (2004).
- [22] S. Y. Lin and H. Guo, *J. Phys. Chem. A* 108, 10066 (2004).
- [23] S. Y. Lin and H. Guo, *J. Phys. Chem. A* 108, 2141 (2004).
- [24] S. Joseph and A. J. C. Varandas, *J. Phys. Chem. A* 113, 4175 (2009).
- [25] A. J. C. Varandas, *J. Mol. Struct.: THEOCHEM.* 120, 401 (1985)..
- [26] A. J. C. Varandas, *Adv. Chem. Phys.* 74, 255 (1988).
- [27] A. J. C. Varandas, *Chem. Phys. Lett.* 194, 333 (1992).
- [28] A. J. C. Varandas and A. I. Voronin, *Mol. Phys.* 85, 497 (1995).
- [29] A. J. C. Varandas, *Lecture Notes in Chemistry*; A. Laganá, A. Riganeli, Eds. Springer: Berlin 75, 33 (2000).
- [30] S. Joseph and A. J. C. Varandas, *J. Phys. Chem. A* 114, 2655 (2010).
- [31] P. Defazio, C. Petrongolo, B. Bussery-Honvault, and P. Honvault, *J. Chem. Phys.* 131, 114303 (2009).
- [32] P. Defazio, P. Gamallo, M. Gonzalez, S. Akpınar, B. Bussery-Honvault, P. Honvault, and C. Petrongolo, *J. Chem. Phys.* 132, 104306 (2010).
- [33] J. Liu, B. Fu, and D. Zhang, *Chem. Phys. Lett.* 480, 46 (2009).
- [34] K. H. Becker, B. Engelhardt, P. Wiesen, and K. D. Bayes, *Chem. Phys. Lett.* 154, 342 (1989).
- [35] A. J. Dean, D. F. Davidson, and R. K. Hanson, *J. Phys. Chem.* 95, 183 (1991).
- [36] A. J. Dean and R. K. Hanson, *Int. J. Chem. Kinet.* 24, 517 (1992).
- [37] L. B. Harding, R. Guadagnini, and G. C. Schatz, *J. Phys. Chem.* 97, 5472 (1993).

- [38] R. van Harrevelt, M. C. van Hemert, and G. C. Schatz, *J. Chem. Phys.* 116, 6002 (2002).
- [39] P. Gamallo, P. Defazio, S. Akpınar, and C. Petrongolo, *J. Phys. Chem. A* 116, 8291 (2012).
- [40] R. F. Lu, T. S. Chu, and K. L. Han, *J. Phys. Chem. A* 109, 6683 (2005).
- [41] R. F. Lu, T. S. Chu, Y. Zhang, K. L. Han, A. J. C. Varandas, and J. Z. H. Zhang, *J. Chem. Phys.* 125, 133108 (2006).
- [42] R. F. Lu, P. Y. Zhang, T. S. Chu, T. X. Xie, and K. L. Han, *J. Chem. Phys.* 126, 124304 (2007).
- [43] D. H. Zhang, J. Z. H. Zhang, Y. C. Zhang, D. Y. Wand, and Q. G. Zhang, *J. Chem. Phys.* 102, 7400 (1995).
- [44] T. S. Chu, R. F. Lu, and K. L. Han, *J. Chem. Phys.* 122, 244322 (2005).
- [45] R. F. Lu, Y. H. Wang, and K. M. Deng, *J. Comput. Chem.* 34, 1735 (2013).
- [46] A. J. H. M. Meijer and E. M. Goldfield, *J. Chem. Phys.* 108, 5404 (1998).
- [47] A. J. H. M. Meijer and E. M. Goldfield, *J. Chem. Phys.* 110, 870 (1999).
- [48] T. E. Carroll and E.M. Goldfield, *J. Phys. Chem. A* 105, 2251 (2001).
- [49] T. S. Chu and K. L. Han, *Phys. Chem. Chem. Phys.* 10, 2431 (2008).
- [50] E. L. Wu, *J. Comput. Chem.* 31, 2827 (2010).